

The corrosion behavior of 316L stainless steel additively manufactured by direct energy deposition process

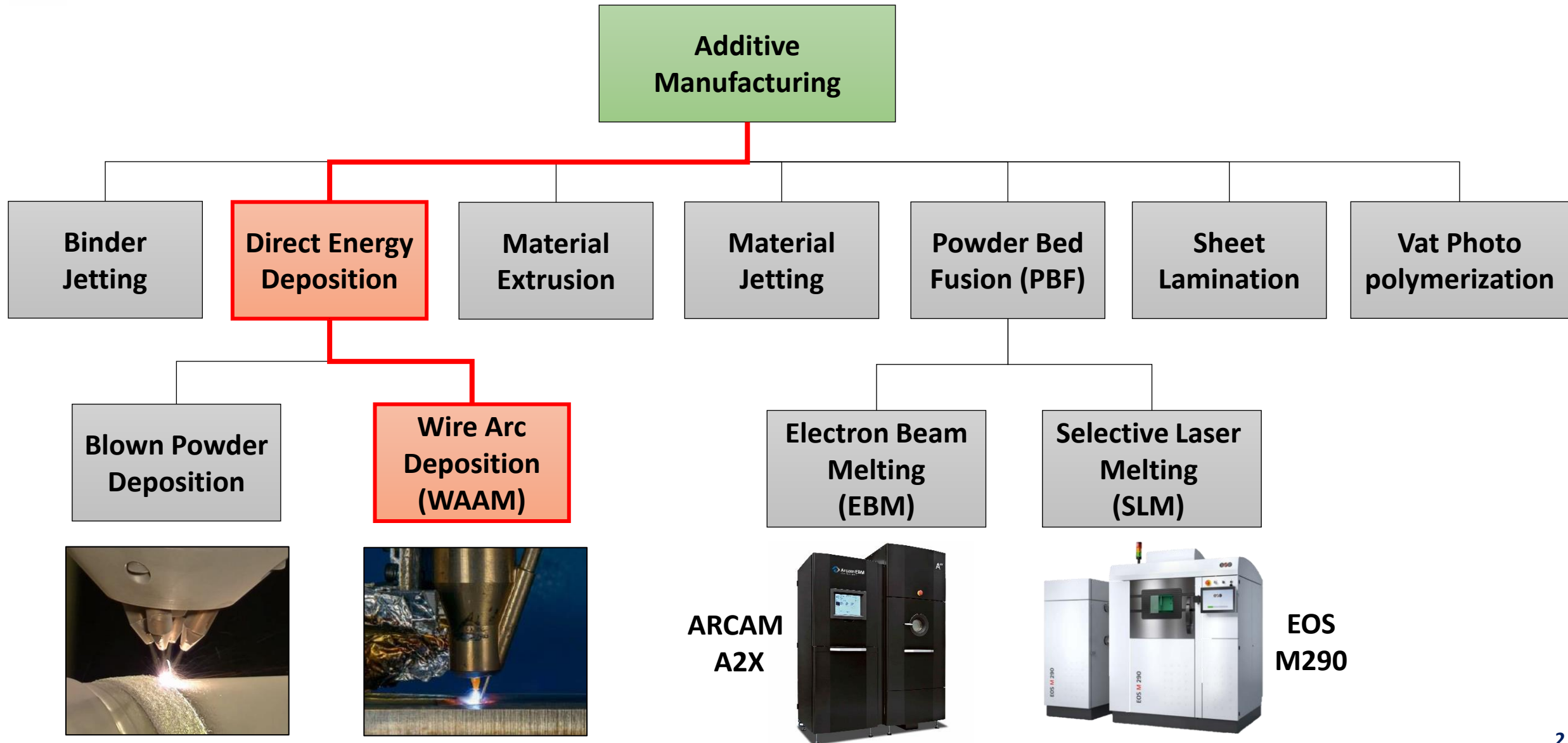
Tomer Ron*, Avi Leon, Amnon Shirizly and Eli Aghion

Department of Materials Engineering, Ben-Gurion University of the Negev, Beer-Sheva, Israel

*Corresponding author: toron@post.bgu.ac.il



Additive Manufacturing (3D printing) Technologies





Relative benefits and limitations of WAAM

	PBT	WAAM
Cost	High ✗	Low ✓
Energy consumption	High ✗	Low ✓
Deposition rate	Low ✗	High ✓
Dimensions	Limited ✗	Unlimited ✓
Surface roughness	Low ✓	High ✗
Compellability	High ✓	Low ✗

Numerical example (stainless steel)

Process parameters	SLM	WAAM
Deposition rate (Kg/h)	0.4	10
Power (KW/Kg)	62.9	5.18
Raw material (\$/Kg)	97	15
Total cost (\$/Kg)	1140	160



Materials and methods

Microstructure

Optical
Microscopy

SEM

XRD

Mechanical properties

Tensile

Corrosion and stress corrosion performance

Immersion

SSRT

Polarization

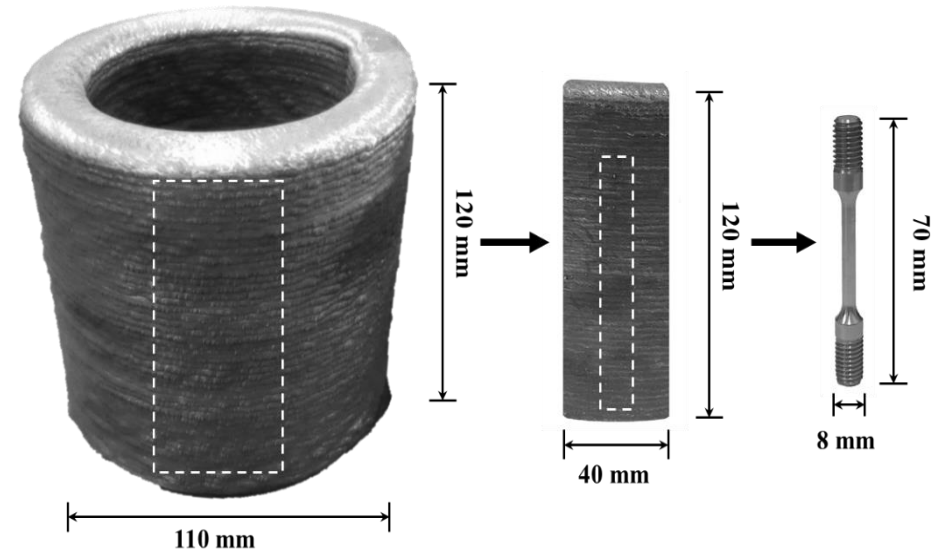
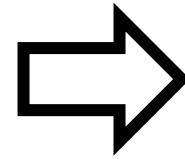
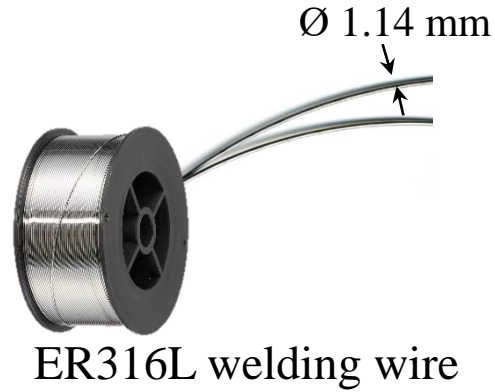
Impedance



Wire Arc Deposition - WAAM of ER70S and 316L



Cloos Rotrol V7.13



Deposition parameter:

Layer thickness: 2 mm

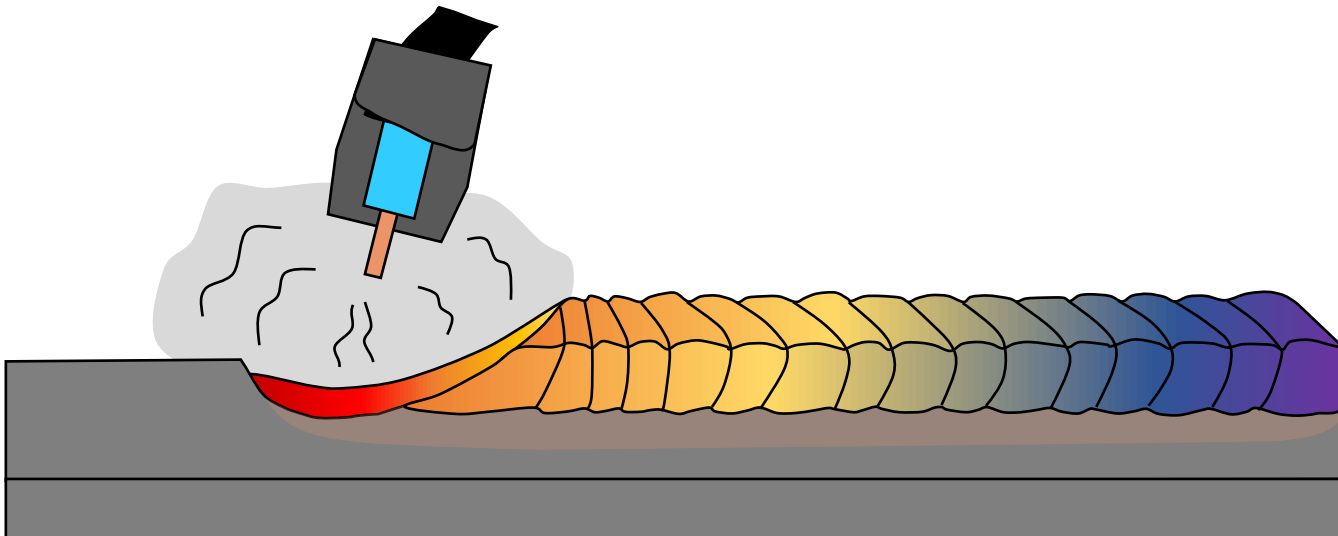
Deposition speed: 14 cm/min

Feed rate: 6.1 m/min

Pulse frequency: 120 Hz

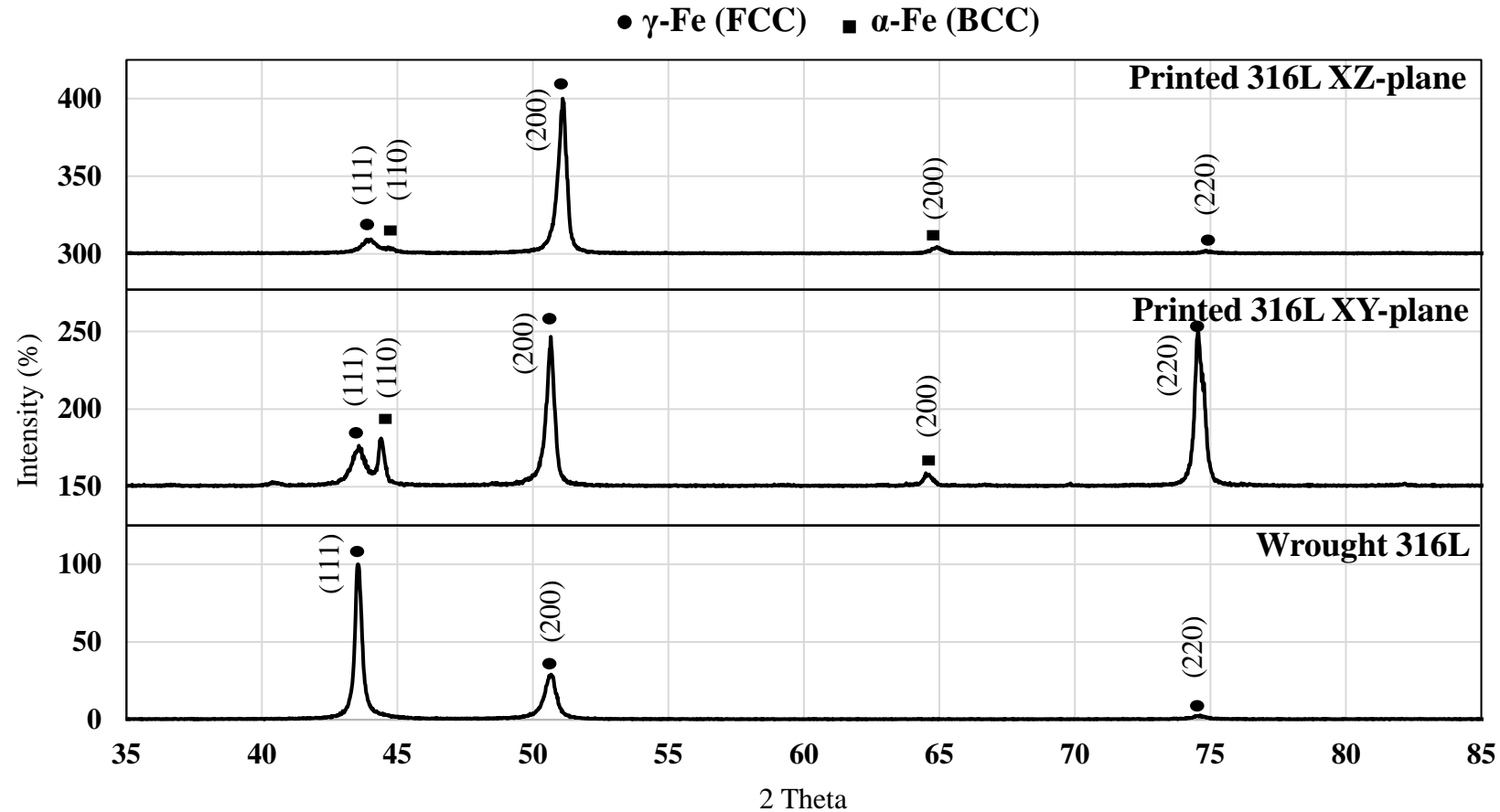
Current: 210 A

Voltage: 23.9-24.1 V





X-ray diffraction

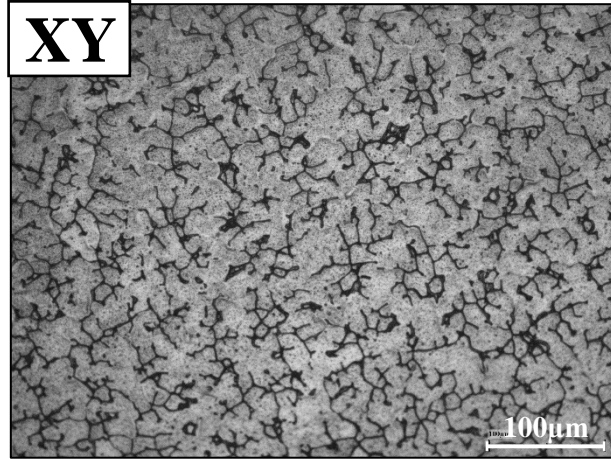


- Wrought alloy: single phase, γ -Fe (FCC).
- Printed alloy: γ -Fe (FCC) matrix and secondary δ -Fe (BCC).
- The difference between the peaks intensities of the printed alloy in the XY and XZ planes relates to the epitaxial solidification of the alloy.

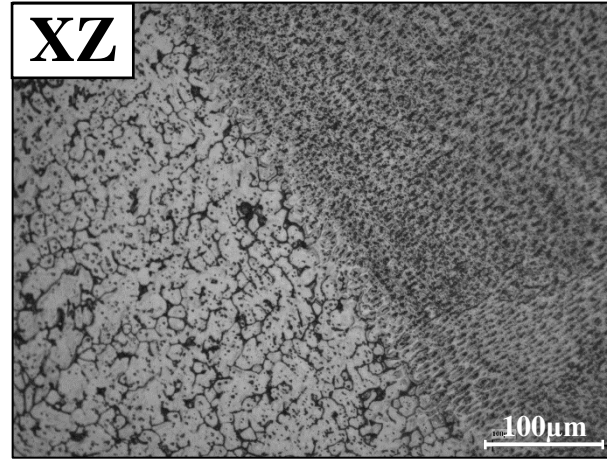


Microstructure of printed 316L obtained by WAAM process

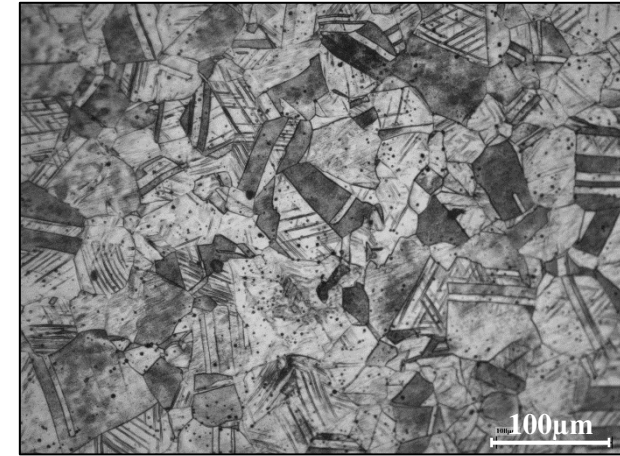
Printed 316L



Fe-0.024%C-19.21%Cr-11.62%Ni



Wrought 316L

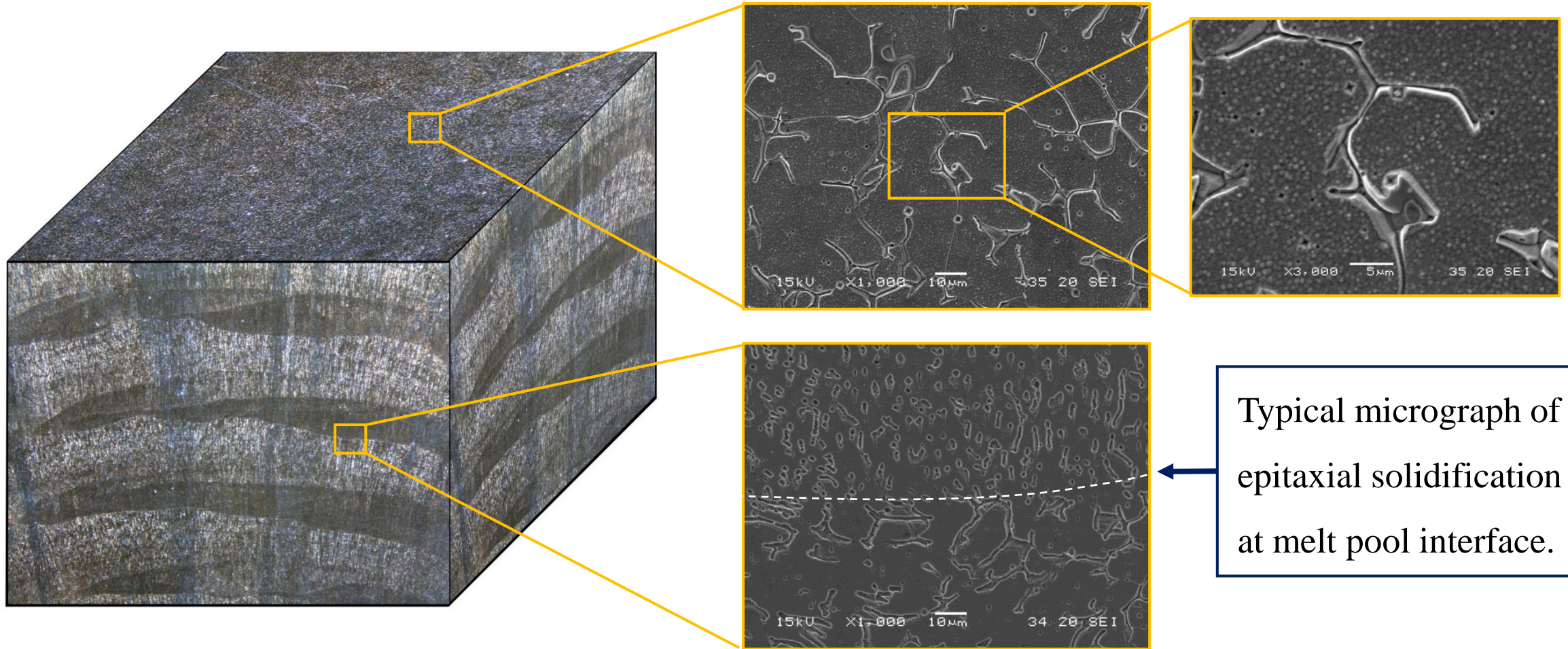


Fe-0.021%C-16.58%Cr-10.07%Ni

- The microstructure of the printed 316L was composed of austenitic matrix and secondary ferritic phase. This was in contrast with the wrought alloy that was composed only from austenitic phase.
- There was a difference between the transverse and longitudinal cross-sections of the printed 316L. This was illustrated by the presence of melt pool boundaries in XZ orientation.



Close-up view of macro and microstructure of printed 316L





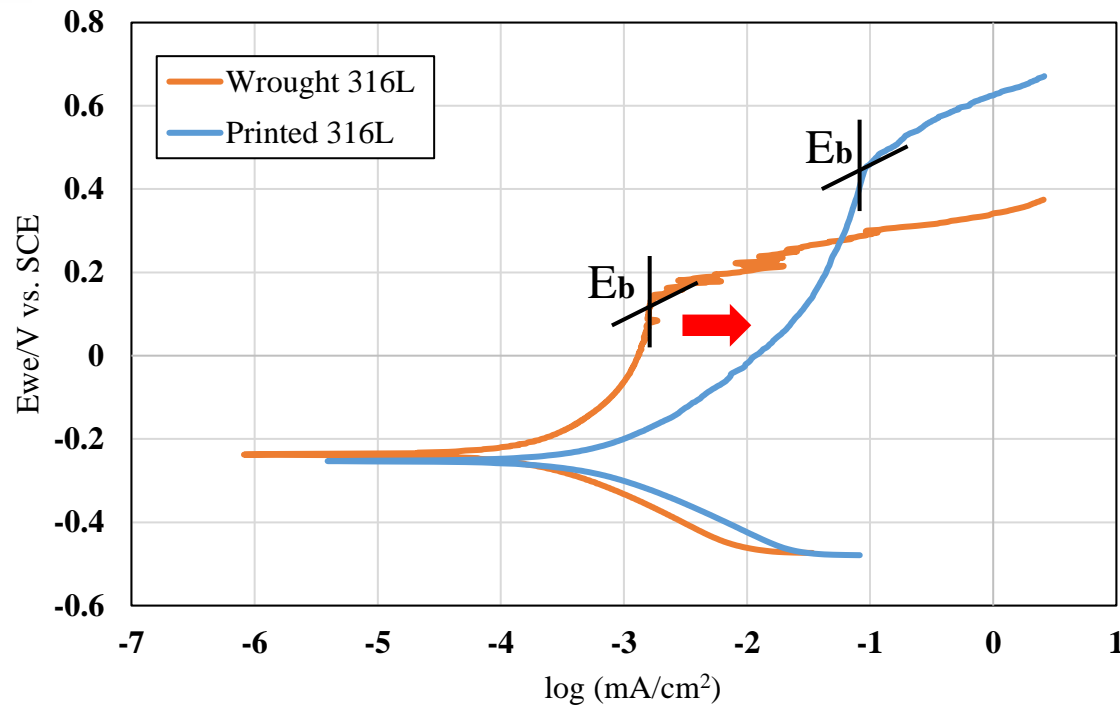
Mechanical properties

Mechanical properties	Printed 316L	AISI 316L
Yield Strength (MPa)	364±17	695±3
Tensile Strength (MPa)	552±11	752±3
Elongation (%)	52±1	37±1
Hardness (HV)	196±5	275±9

- The strength and hardness of the printed alloy were relatively reduced compared to the counterpart 316L alloy, while the ductility was comparatively increased.



Potentiodynamic polarization



- The passivation transition curves of the two alloys were relatively similar with different break potential and corrosion current.
- Although Tafel extrapolation showed that the corrosion rate of the printed alloy was relatively higher than the wrought alloy, both alloys exhibit outstanding corrosion resistance (<0.02 mm/yr).

	Printed 316L	Wrought 316L
E_{Corr} (v)	-0.25 ± 0.02	-0.21 ± 0.02
I_{Corr} (μA)	0.48 ± 0.12	0.09 ± 0.004
Corrosion rate (mmpy)	0.005 ± 0.001	0.001 ± 0.001
E_{break} (v)	0.47 ± 0.03	0.13 ± 0.04

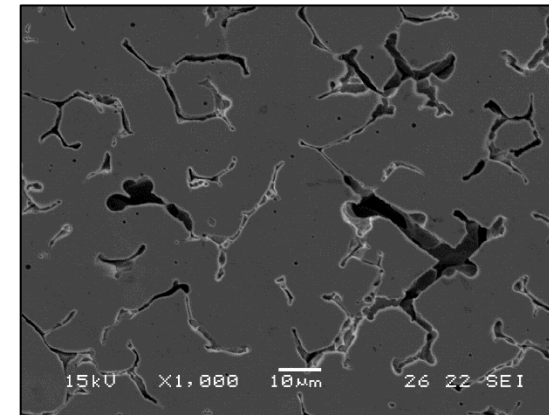
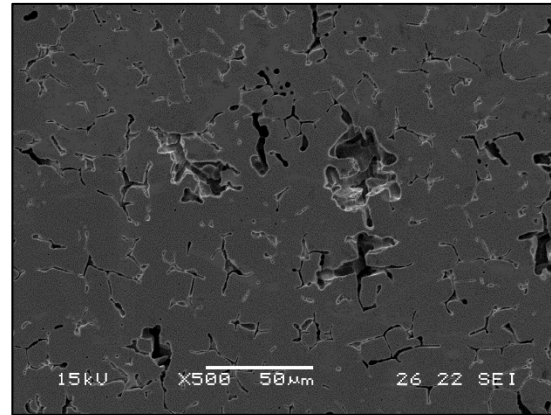
Corrosion rate (mm/yr)	
Outstanding	< 0.02
Excellent	0.02 – 0.1
Good	0.1 – 0.5
Fair	0.5 - 1
Poor	1 - 5
Unacceptable	> 5



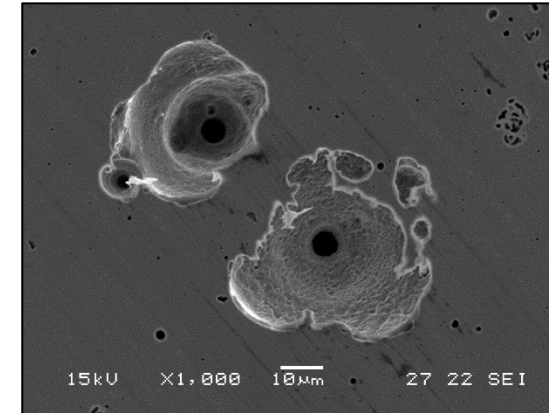
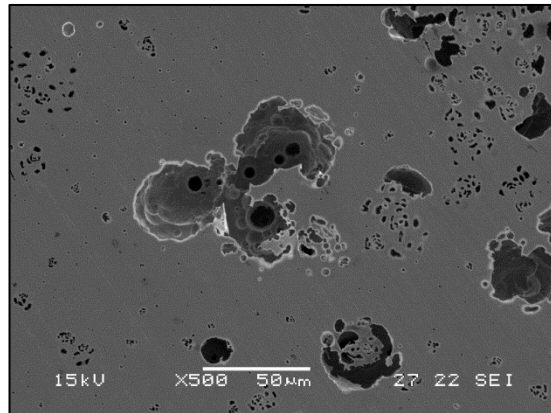


Localized corrosion attack

**Printed
316L**



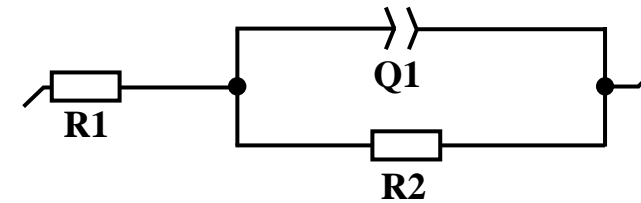
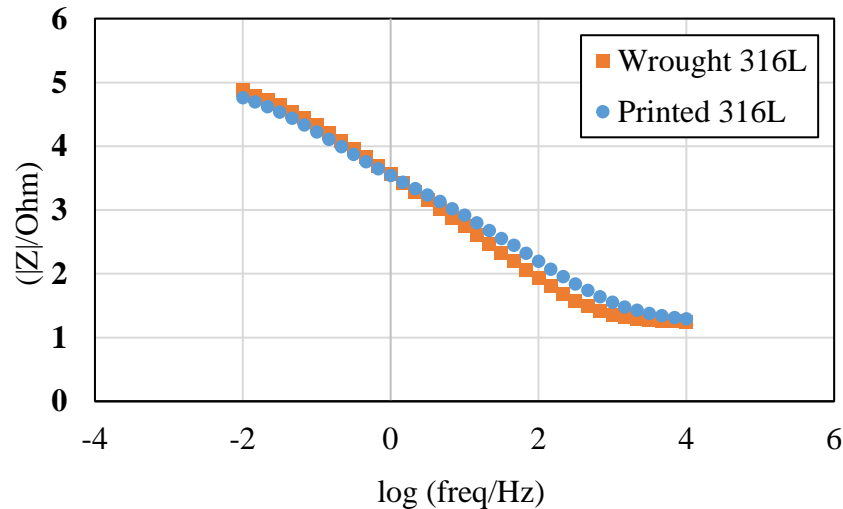
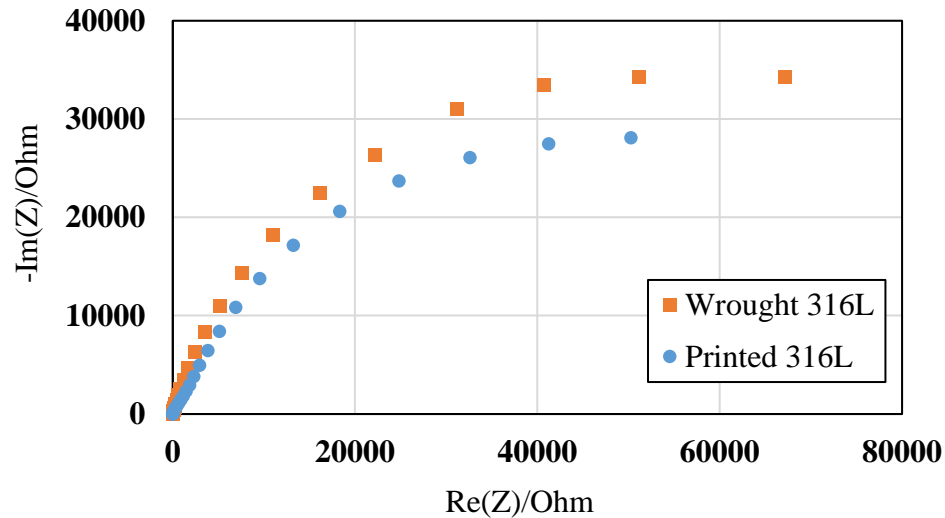
**Wrought
316L**



- As expected from active - passive polarization curve, both alloys presented pitting corrosion attack.
- While the pitting corrosion attack in the wrought alloy was relatively scattered, this attack was more intense in the printed alloy at the interface between the austenitic matrix and the ferritic phase.



Impedance spectroscopy

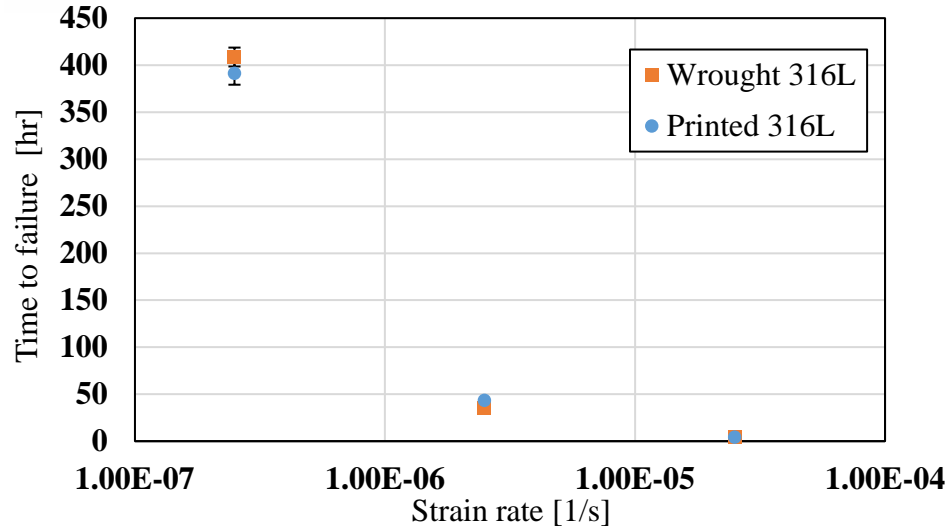


	R1 (Ohm)	Q1 ($F.s^{(a-1)}$)	a	R2 (Ohm)
Printed 316L	15.6	7.31E-5	0.705	92,178
Wrought 316L	16.98	6.07E-5	0.825	83,863

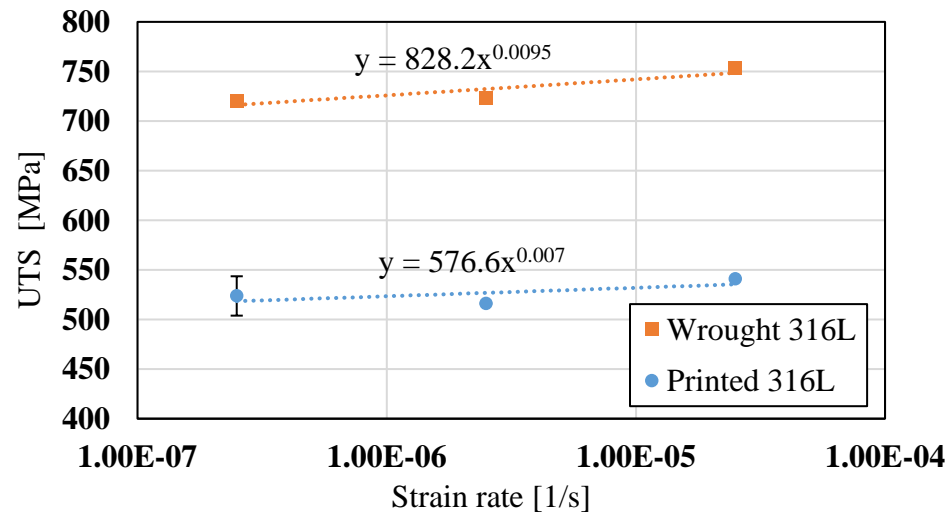
- The differences between the two alloys in terms of impedance examination were minor and in accord the results obtained by the potentiodynamic polarization analysis.



Slow Strain Rate Tasting (SSRT)

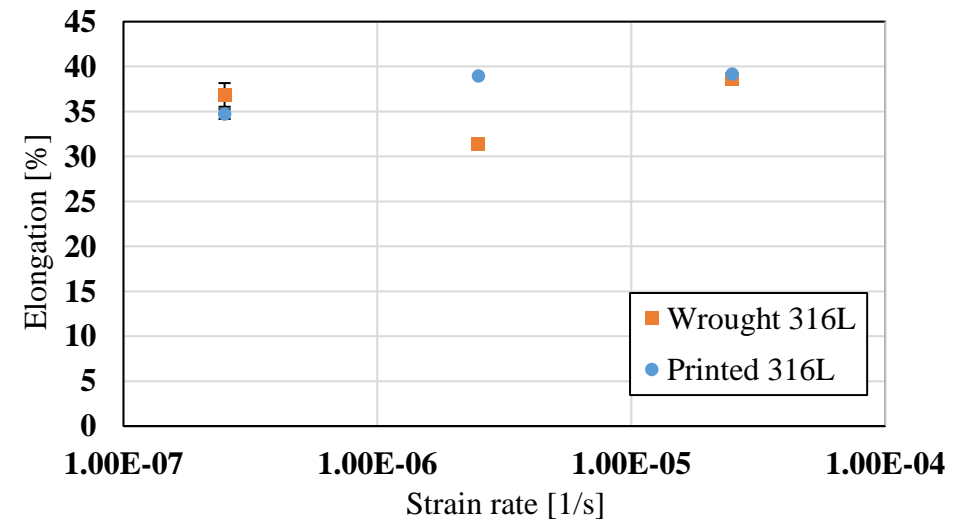


- The differences in UTS and elongation between the two alloys comes in line with their inherent differences in mechanical properties.
- The stain rate sensitively factors (m) of the two alloys were very close. This indicated that their stress corrosion sensitivity was similar as demonstrated by nearly equal time to failure.



$$\sigma_{UTS} = C \cdot \dot{\epsilon}^m$$

m - Strain rate sensitivity factor





Conclusions related to printed 316L alloy

1. The corrosion performance of the printed 316L obtained by a WAAM process was quite similar to its counterpart wrought alloy.

In both cases the corrosion resistance was excellent as expected from austenitic stainless steel.

2. The stress corrosion resistance of the printed 316L and wrought alloy in terms SSRT analysis were similar apart from their inherent differences in mechanical properties.

General conclusion

The promising results of WAAM with ferrous alloys can pave the road for future WAAM applications using refractory metals such as Tantalum and Tungsten as raw material.



Related Publications

1. **T. Ron**, O. Dolev, A. Leon, A. Shirizly and E. Aghion “Effect of Phase Transformation on Stress Corrosion Behavior of Additively Manufactured Austenitic Stainless Steel Produced by Directed Energy Deposition”. *Materials*, 2021 14(1), 55;
2. **T. Ron**, G. K Levy, O. Dolev, A. Leon, A. Shirizly and E. Aghion "The Effect of Microstructural Imperfections on Corrosion Fatigue of Additively Manufactured ER70S-6 Alloy Produced by Wire Arc Deposition" *Metals* Jan. 2020.
3. **T. Ron**, G. K Levy, O. Dolev, A. Leon, A. Shirizly and E. Aghion "Environmental behavior of low carbon steel produced by a wire arc additive manufacturing process" *Metals*, 2019, 9, 888.



**Thank You for
Your Attention!**